Modification of porous nickel electrodes with silver nanoparticles for hydrogen production

V. Pérez-Herranz[a*], R. Medina[b], P. Taymans[c], C. González-Buch[a], E. M. Ortega[a], G. Sánchez-Loredo[d], G. J. Labrada-Delgado[e].

[a]Departamento de Ingeniería Química y Nuclear, E.T.S.I. Industriales, Universitat Politècnica de València. P.O. Box 22012, E-46071 Valencia, Spain

[b]Universidad Politécnica de San Luis Potosí, Urbano Villalón 500, La Ladrillera, 78369, San Luis Potosí, México

[c]Institut Supérieur Industriel de Bruxelles. Haute Ecole Paul-Henri Spaak, Bruxelles, Belgium.

[d]Instituto de Metalurgia/Facultad de Ingeniería, Universidad Autónoma de San Luis Potosí, Sierra Leona 550, 78210, San Luis Potosí, México.

[e]Instituto Potosino de Investigación Científica y Tecnológica, Camino a la Presa San José 2055, 78216, San Luis Potosí, México.

[*]Corresponding author: vperez@iqn.upv.es (V. Pérez-Herranz)

Absract.

Silver nanoparticles were electrodeposited into the surface of a macroporous Ni electrode. The developed electrodes were characterized morphologically by confocal laser scanning microscopy and field emission scanning electron microscopy. The activity of the developed electrodes towards the hydrogen evolution reaction was assessed by pseudo-steady-state polarization curves and electrochemical impedance spectroscopy in alkaline solutions at different temperatures. The incorporation of the silver nanoparticles on the surface of the electrode improved the catalytic activity towards the hydrogen evolution reaction due to an improvement in the electrochemically active surface area rather than in the intrinsic catalytic activity.

Key words: Porous electrodes; Ag nanoparticles; HER; EIS

1. Introduction.

Actually, about 81% of the primary world energy production comes from fossil fuels. However, fossil fuels are not reliable because their use leads to serious environmental problems derived from the greenhouse effect and due to the exhaustion of reserves [1]. Hydrogen can be considered an alternative to fossil fuels that meets all the criteria for an alternative clean energy source because it is versatile, environmentally compatible and it could be produced from renewable energy sources. However, hydrogen is not found in pure form on Earth, so it should be considered an energy carrier or storage medium rather than an energy source, and the climate change impact of using it depends on the raw material used for its production [1,2].

Alkaline water electrolysis is one of the most promising methods for hydrogen production, as it is environmentally friendly when combined with renewable energy sources such as wind or solar [3,4]. However, the use of this technique to produce hydrogen on a large scale is restricted by its high costs, both economic and energetic, the latter derived from the high overvoltages necessary to carry out the water oxidation and reduction reactions taking place at the electrodes. Noble metals such as Pt, Ir or Pd have the highest catalytic activity for both, the hydrogen evolution reaction (HER) and the oxygen evolution reaction (OER), and Ni is the most active non-noble elemental electrocatalyst for HER in alkaline solutions [5,6].

The catalytic activity of an electrode can be increased by enlarging its real surface area and/or increasing its intrinsic activity. The increase of the active surface of the electrodes can be achieved by the utilization of Raney-type alloys [6–8], by electrodeposition at high current densities [9–11] or by means of electrodeposition on templates [12,13]. In order to improve the intrinsic catalytic activity, Ni-based alloys such as NiAl [14], NiZn [15,16], NiMo [17,18] NiCo [9,10,19–22], NiFe [23,24], NiCu [25,26], NiW [27,28] or modified electrodes [29–31] have been studied.

Recently, there has been a great interest in the development of nanostructured metallic materials to be used as electrocatalysts, since these materials have properties remarkably different from their bulk counterparts. In addition, small amounts of

material are used and they provide a high surface area. In this way, different nanostructured materials have been used as electrocatalysts for water oxidation and reduction [32–38]. The catalytic activity of the nanoparticles depends on the preparation method [32]. In the case of silver nanoparticles, several methods, such as chemical reduction using a variety of organic and inorganic reducing agents, electrochemical methods, physicochemical reduction and radiolysis, have been used for their synthesis [33,39–41].

In this work, silver nanoparticles (AgNPs) were electrodeposited on Ni macroporous substrates to produce AgNP-modified Ni electrodes as effective electrocatalysts for the HER. The use of a macroporous electrode as a supporting material can reduce the dosage of noble metals. The resulting morphologies were characterized by confocal laser scanning microscopy and field emission scanning electron microscopy. The electrocatalytic activity of the synthesized catalysts towards the HER was studied in alkaline solution under various experimental conditions by pseudo-steady-state polarization curves and electrochemical impedance spectroscopy (EIS).

2. Experimental.

2.1. Modification of the macroporous Ni electrodes with AgNPs.

Macroporous Ni electrodes were obtained by means of electrodeposition at high current densities on a stainless steel AISI 304 substrate as described in our previous works [10,38]. Then, silver nanoparticles were electrodeposited under different conditions from a 50 mL solution of 0.5 mM $AgNO_3$ in distilled water. The electrodeposition process begins by applying a ramp of current density for a time, t_{ramp}, until a maximum current density of 1 $A \cdot m^{-2}$ is reached, and then this maximum current density is maintained for a time, t_{const}. The operating conditions for the modification of the macroporous nickel electrodes are shown in Table 1. In this table, it is also shown the maximum loadings of Ag nanoparticles assuming that the electrodeposition current efficiency was 100%. The surface morphologies of the developed electrodes were studied by means of an OLYMPUS LEXT OLS3100-USS confocal laser scanning microscope, and a ZEISS ULTRA 55 field emission scanning electron microscope (FE-SEM) coupled with an Energy-Dispersive X-Ray (EDX) analysis was used to observed the morphology and to confirm the presence of the Ag nanoparticles on the electrode surface.

2.2. Elecrochemical measurements.

Pseudo-steady-state polarization curves and EIS techniques were used to characterize the developed electrodes towards the HER. All the experiments were performed in oxygen free 30 wt.% KOH solutions which were achieved by bubbling N_2 for 15 min.

The pseudo-steady-state polarization curves were potentiodynamically recorded at a scan rate of 1 $mV \cdot s^{-1}$ from -1.60 V vs. Ag/AgCl (-1.40 V vs. SHE) until the equilibrium potential. These curves were obtained at different temperatures from 30 to 80 ºC. Before the experiments, the working electrode was held at -1.60 V vs. Ag/AgCl in the same solution, for the time needed to set up reproducible polarization curves.

EIS measurements were recorded after the corresponding polarization curves at different cathodic overpotentials from 0 to 100 mV in the frequency range of 10 kHz to 5 mHz, with ten frequencies per decade and a sinusoidal signal of 10 mV peak-to-peak. The complex nonlinear least square (CNLS) fitting of the impedance data was carried out with the ZView 3.0 software package.

The electrochemical measurements were carried out in an electrochemical cell developed by the Dpto. Ingeniería Química y Nuclear of the Universitat Politècnica de Valencia (Spain) described in previous works [10,11,20].

3. **Results and discussion.**

3.1. Morphology characteriation.

Figure 1 shows the FE-SEM (A) and confocal laser micrographs (B) of the macroporous Ni electrode without AgNPs. As can be seen the electrode surface structure consists of a continuous matrix provided by circular macropores evenly distributed on the whole surface. This structure is a consequence of the high current densities applied originated by the random nucleation of the dissolved hydrogen, which produces microbubbles attached to the electrode surface, as it has been previously reported [13,22,38,42]. No significant differences were observed in this porous macrostructure due to the deposition of AgNPs.

Figure 2 shows the surface morphology of the Ag nanoparticles deposited on the surface of the macroporous Ni electrodes. In the electrodes E1 and E2 (Figure 2 A and B respectively), obtained by electrodeposition, it is observed that for the same applied electric charge of $3.25 \cdot 10^{-3}$ C, dispersed spherical AgNPs of about 50 nm, and some aggregation of such nanoparticles was observed. The amount of deposited nanoparticles was greater at electrode E2, where the duration of the applied current density ramp was higher. In the case of electrode E3, obtained with the highest applied electric charge, the nanoparticles showed dendritic growth (Figure 2 C).

3.2. Polarization measurements.

The electrocatalytic activity of the Ni-AgNP developed electrodes towards the HER was studied by means of pseudo-steady-state polarization curves and EIS and was compared with a macroporous Ni electrode without AgNPs.

Figure 3 shows the cathodic polarization curves recorded in a 30 wt% KOH solution at 50 °C on the developed electrodes. The curves were corrected with respect to the reversible HER potential at the given conditions and for the *jR*-drop. All curves present a linear behaviour at high overpotentials, indicating that the HER on the developed electrodes is kinetically controlled and can be described by the Tafel equation:

$$\eta = a + b \log j \quad (1)$$

where η (V) is the overpotential, j (A·cm^{-2}) is the measured current density, b (V decade^{-1}) is the Tafel slope and a (V) is the intercept, which is related to the exchange current density, j_0 (A·cm^{-2}) through the equation:

$$a = \frac{2.3\ RT}{\alpha\ F} \log j_0 \quad (2)$$

where R is the gas constant, F is the Faraday constant, and α is the charge transfer coefficient, which can be calculated from the Tafel slope:

$$b = -\frac{2.3\ RT}{\alpha\ F} \quad (3)$$

From the fitting of the linear part of the Tafel curves shown in Figure 3 it is possible to determine the kinetic parameters a, b, j_0 and α. The values of the kinetic parameters are reported in Table 2. In this table, it is also reported the overpotential at a fixed current density of 100 mA·cm^{-2}, η_{100}. This parameter is an indication of the energy that has to be invested to produce a fixed amount of hydrogen. For a given electrode, the lower the overpotential at a fixed current density, the higher the catalytic activity of the electrode.

As can be concluded from the Tafel curves shown in Figure 3 and from the values of the kinetic parameters shown in Table 2, the electrodes modified with AgNPs show the best performance, and therefore the higher catalytic activity to the HER, since they present higher values of j_0 and lower values of η_{100} than the macroporous electrode without AgNPs. With respect to the electrodes modified with silver nanoparticles, electrodes E1, E2 and E3, it can be seen that the catalytic activity with respect to the HER improves with the increase of the electric charge, and therefore with the amount of silver nanoparticles electrodeposited on the macroporous structure. The electrodes E1 and E2, in which the same amount of silver has been electrodedeposited, present similar values of the kinetic parameters j_0 and η_{100}, and the electrode E3 shows the highest catalytic activity with respect to the HER, since it provides the highest j_0 and the lowest η_{100} values. The influence of temperature on the values of the kinetic parameters is significant. The exchange current densities, j_0, increase, which is the expected behaviour.

Since all electrodes have similar values of Tafel slope, the same HER reaction mechanism should be valid for the developed electrodes. The commonly accepted

mechanism of HER in alkaline solutions involves the following steps: formation of an adsorbed hydrogen adatom intermediate (Volmer reaction, eq. (4)) followed by either the electrochemical desorption of hydrogen into solution (Heyrovsky reaction, eq. (5)) and/or a chemical hydrogen desorption by the combination of two adatoms (Tafel reaction, eq. (6)).

$$H_2O + M + e^- \rightarrow MH_{ads} + OH^- \quad (4)$$

$$H_2O + MH_{ads} + e^- \rightarrow H_2 + M + OH^- \quad (5)$$

$$MH_{ads} + MH_{ads} \rightarrow H_2 + 2M \quad (6)$$

where M is a free site on the metal surface and MH_{ads} is the metal surface occupied by hydrogen adatoms.

As it can be seen from Table 2, the Tafel slope values vary between 90 and 140 $mV \cdot dec^{-1}$ at 30 and 50 ºC respectively, and the charge transfer coefficient is around 0.5 for all the electrodes. Then, according to the literature of HER on transition metals, it can be concluded that the HER on the developed electrodes takes place by means of the same Volmer-Heyrovsky mechanism [5,43,44].

In order to perform a complete characterization of the processes taking place at the electrode/electrolyte interface, EIS measurements were made at different overpotentials selected from the previous polarization curves. Figures 4 and 5 show the impedance response of electrode E1 by means of the Nyquist and Bode diagrams at different overvoltages and temperatures respectively, while in Figure 6 is represented the impedance response of all the developed electrocatalysts at a given overvoltage and temperature. The behavior observed at high frequencies, independent of both temperature and overpotential (see inset of Figures 4 A and 5 A), is related to a cylindrical pore geometry of finite-length pores, as it was observed in the morphology study, with no mass transfer effects [10]. On the other hand, as can be seen in Figure 4, the diameter of the two semicircles observed in the complex plane plot decreases as the cathodic overpotential increases. The same phenomenon was observed with the increase in the temperature (Figure 5), indicating that both time constants are related to the electrode kinetics [13,45]. This behavior was observed for all the developed electrodes. In all the cases, at the higher overpotential applied, HER is so vigorous that hydrogen

bubbles cause too much interference, good impedance spectra could not be obtained and only one deformed semicircle was observed. This same phenomenon has been observed by other authors [6,10].

In order to model the behavior of the impedance obtained, and depending on the observed behavior, the electric equivalent circuits (EEC) presented in Figure 7 were used. When the impedance response is characterized by two overlapped semicircles in the Nyquist plot, and taking into account the behavior of both semicircles with the overpotential and with the temperature previously described, the two-time constant parallel (2TP) EEC model shown in Figure 7 A was used to fit the EIS response of the investigated electrocatalysts. In this model, initially proposed by Armstrong and Henderson [30], the high frequency time constant, τ_{HF}, is related to the charge transfer kinetics, and the low frequency time constant, τ_{LF}, is associated to the hydrogen adsorption [20,22,45]. On the other hand, when the impedance response is characterized by one semicircle in the Nyquist plot (i.e. impedance response recorded at the highest overpotentials), the experimental data were fitted to the one-time constant (1T) EEC model shown in Figure 7 B. In this case, the semicircle related to the hydrogen adsorption apparently completely disappears and only the semicircle related to the charge transfer is observable. This is because at high overpotentials the adsorption process is facilitated and the impedance response is dominated by the charge transfer process, and the HER is controlled by the Heyrovsky step [20,46,47]. For both EEC models, the double layer capacitance (C_{dl}) was replaced by a constant phase angle element (CPE) [5,45] whose impedance is given by the following equation:

$$Z_{CPE} = [Q \cdot (i \cdot w)^n]^{-1} \quad (7)$$

were Q is the CPE constant, w is the angular frequency (in rad s^{-1}), i^2=-1 is the imaginary number, and n is the CPE exponent.

As can be seen in Figures 4-6 a very good agreement between the experimental data (symbols) and the models was obtained. Table 3 show the best-fit estimates of the different EEC parameters obtained from the impedance measurements of the developed electrodes at different overpotentials and temperatures. The average double layer capacitances, C_i, for the catalysts were determined using the relation suggested by Brug et al. [48]:

$$C_i = \left[Q_i/(R_S^{-1} + R_i^{-1})^{(1-n_i)}\right]^{1/n_i} \quad (8)$$

As can be seen in Table 3, the parameters of the high frequency semicircle, C_1 and R_1 decrease with the cathodic overpotential and with the temperature, indicating an improvement of the HER. This is typical of a charge-transfer process. With respect to the low frequency semicircle, R_2 decreases with the cathodic overpotential and temperatura, while C_2 increases. This behavior being typical of adsorption processes on the electrode surface [44,45,47].

The impedance results, in addition to the information on the kinetics of the HER, can be used to estimate the real active surface area of the developed electrocatalists, in terms of the roughness factor, R_f, by comparing the C_{dl} related to the HER charge-transfer kinetics (C_1) of the porous electrodes with that of a smooth electrode [13,22]. For this purpose, a value of 20 $\mu F \cdot cm^{-2}$ was considered for the double layer capacitance of a smooth nickel surface, used earlier in the literature [21,43]. The values of the roughness factor are presented in Table 3. Figure 8 shows the electrode R_f as a function of the HER overpotential for the developed electrocatalists at 50 ºC. As can be seen in this figure, the values of R_f decrease when increasing the cathodic overpotential. This has been attributed to a blockage of a fraction of the inner surface of the electrode during HER due to gas bubbles shielding, and hence not electrochemically accessed by the electrolyte [12,22]. On the other hand, the presence of AgNPs increases the reaction surface area. The electrode E1 with a smaller amount of AgNPs has a roughness factor similar to the macroporous Ni electrode, but electrodes E2 and E3, with more nanoparticles on the surface, have a higher roughness factor, especially electrode E3 in which the nanoparticles presented dendritic growth.

With the roughness factor values, the effective surface area, A_{eff}, can be calculated as:

$$A_{eff} = A \cdot R_f \quad (9)$$

where A is the geometric area.

Then, the relative intrinsic catalytic activity of the investigated electrodes can be evaluated, by substracting the effect of the surface area. For this purpose, the current density, *j'*, based on the effective surface area can be determined as:

$$j' = \frac{I}{A_{eff}} \tag{10}$$

where *I (A)* is the current.

Figure 9 shows the Tafel plots normalized to the effective surface area. As can be seen in Figure 9, the Tafel curves corrected with respect to the effective surface area for all the developed electrodes are quite similar, indicating that the AgNPs mainly affect the electrochemically active surface area rather than the intrinsic catalytic activity. By the deposition techniques used, the amount of nanoparticles deposited on the macroporous Ni electrode is very small, so the deposited AgNPs have more effect on the electrochemically active surface than on the intrinsic catalytic activity of the electrode.

4. **Conclusions.**

Ni macroporous electrodes were synthesized at high current densities. These macroporous electrodes were modified with silver nanoparticles to evaluate their electrocatalytic activity towards the HER in alkaline solutions by means of pseudo-steady-state polarization curves and EIS.

Silver nanoparticles were successfully electrodeposited on macroporous nickel electrodes. The morphology of the nanoparticles obtained by electrodeposition was affected by the applied electric charge. For low applied electrical charges, spherical nanoparticles were uniformly distributed on the electrode surface, while for high applied electric charges, the nanoparticles showed dendritic growth.

The results about the electrochemical characterization of the developed electrodes by means of polarization curves and EIS indicate that the HER on these electrodes takes place via Volmer-Heyrovsky mechanism. EIS results suggested that the improvement in the HER electrocatalytic activity observed for the AgNPs modified electrodes is mainly due to the increased surface area rather than to an increase on the intrinsic catalytic activity.

5. **Acknowledgements.**

This work was partially supported by the Fondo FONSEC-SRE México-Argentina en Nanotecnología (CONACyT-ANPCYT), Projects 0191145-PICT2012-3081. Ramiro Medina wish to thank to the CONACYT for the postgraduate grant (304413+Beca mixta).

6. References.

[1] F. Barbir, Transition to renewable energy systems with hydrogen as an energy carrier, Energy. 34 (2009) 308–312. doi:10.1016/j.energy.2008.07.007.

[2] M. Momirlan, T.N. Veziroglu, The properties of hydrogen as fuel tomorrow in sustainable energy system for a cleaner planet, Int. J. Hydrogen Energy. 30 (2005) 795–802. doi:10.1016/j.ijhydene.2004.10.011.

[3] K. Zeng, D. Zhang, Recent progress in alkaline water electrolysis for hydrogen production and applications, Prog. Energy Combust. Sci. 36 (2010) 307–326. doi:10.1016/j.pecs.2009.11.002.

[4] J.H. Williams, A. DeBenedictis, R. Ghanadan, A. Mahone, J. Moore, W.R. Morrow, S. Price, M.S. Torn, The Technology Path to Deep Greenhouse Gas Emissions Cuts by 2050: The Pivotal Role of Electricity, Science (80-.). 335 (2012).

[5] A. Lasia, A. Rami, Kinetics of hydrogen evolution on nickel electrodes, J. Electroanal. Chem. Interfacial Electrochem. 294 (1990) 123–141. doi:10.1016/0022-0728(90)87140-F.

[6] Y. Choquette, L. Brossard, A. Lasia, H. Ménard, Investigation of hydrogen evolution on Raney-Nickel composite-coated electrodes, Electrochim. Acta. 35 (1990) 1251–1256. doi:10.1016/0013-4686(90)90058-8.

[7] P. Los, A. Rami, A. Lasia, Hydrogen evolution reaction on Ni-Al electrodes, J. Appl. Electrochem. 23 (1993) 135–140. doi:10.1007/BF00246950.

[8] C. Hitz, A. Lasia, Experimental study and modeling of impedance of the her on porous Ni electrodes, J. Electroanal. Chem. 500 (2001) 213–222. doi:10.1016/S0022-0728(00)00317-X.

[9] I. Herraiz-Cardona, E. Ortega, L. Vázquez-Gómez, V. Pérez-Herranz, Electrochemical characterization of a NiCo/Zn cathode for hydrogen generation, Int. J. Hydrogen Energy. 36 (2011) 11578–11587. doi:10.1016/j.ijhydene.2011.06.067.

[10] C. González-Buch, I. Herraiz-Cardona, E. Ortega, J. García-Antón, V. Pérez-Herranz, Synthesis and characterization of macroporous Ni, Co and Ni-Co electrocatalytic deposits for hydrogen evolution reaction in alkaline media, Int. J. Hydrogen Energy. 38 (2013) 10157–10169. doi:10.1016/j.ijhydene.2013.06.016.

[11] C. González-Buch, I. Herraiz-Cardona, E. Ortega, J. García-Antón, V. Pérez-Herranz, Study of the catalytic activity of 3D macroporous Ni and NiMo cathodes for hydrogen production by alkaline water electrolysis, J. Appl. Electrochem. 46 (2016) 791–803. doi:10.1007/s10800-016-0970-0.

[12] V. Ganesh, V. Lakshminarayanan, Preparation of high surface area nickel electrodeposit using a liquid crystal template technique, Electrochim. Acta. 49 (2004) 3561–3572. doi:10.1016/j.electacta.2004.03.024.

[13] I. Herraiz-Cardona, E. Ortega, L. Vázquez-Gómez, V. Pérez-Herranz, Double-template fabrication of three-dimensional porous nickel electrodes for hydrogen

evolution reaction, Int. J. Hydrogen Energy. 37 (2012) 2147–2156. doi:10.1016/j.ijhydene.2011.09.155.

[14] L. Wu, Y. He, T. Lei, B. Nan, N. Xu, J. Zou, B. Huang, C.T. Liu, The stability of hydrogen evolution activity and corrosion behavior of porous Ni3Al–Mo electrode in alkaline solution during long-term electrolysis, Energy. 67 (2014) 19–26. doi:10.1016/j.energy.2014.02.033.

[15] G. Sheela, M. Pushpavanam, S. Pushpavanam, Zinc–nickel alloy electrodeposits for water electrolysis, Int. J. Hydrogen Energy. 27 (2002) 627–633. doi:10.1016/S0360-3199(01)00170-7.

[16] R. Solmaz, G. Kardaş, Hydrogen evolution and corrosion performance of NiZn coatings, Energy Convers. Manag. 48 (2007) 583–591. doi:10.1016/j.enconman.2006.06.004.

[17] L.S. Sanches, S.H. Domingues, C.E.B. Marino, L.H. Mascaro, Characterisation of electrochemically deposited Ni–Mo alloy coatings, 2004. doi:10.1016/j.elecom.2004.04.002.

[18] N.V. Krstajić, V.D. Jović, L. Gajić-Krstajić, B.M. Jović, A.L. Antozzi, G.N. Martelli, Electrodeposition of Ni–Mo alloy coatings and their characterization as cathodes for hydrogen evolution in sodium hydroxide solution, Int. J. Hydrogen Energy. 33 (2008) 3676–3687. doi:10.1016/j.ijhydene.2008.04.039.

[19] F.J. Pérez-Alonso, C. Adán, S. Rojas, M.A. Peña, J.L.G. Fierro, Ni–Co electrodes prepared by electroless-plating deposition. A study of their electrocatalytic activity for the hydrogen and oxygen evolution reactions, Int. J. Hydrogen Energy. 40 (2015) 51–61. doi:10.1016/j.ijhydene.2014.11.015.

[20] I. Herraiz-Cardona, C. González-Buch, C. Valero-Vidal, E. Ortega, V. Pérez-Herranz, Co-modification of Ni-based type Raney electrodeposits for hydrogen evolution reaction in alkaline media, J. Power Sources. 240 (2013) 698–704. doi:10.1016/j.jpowsour.2013.05.041.

[21] I. Herraiz-Cardona, E. Ortega, V. Pérez-Herranz, Impedance study of hydrogen evolution on Ni/Zn and Ni-Co/Zn stainless steel based electrodeposits, Electrochim. Acta. 56 (2011) 1308–1315. doi:10.1016/j.electacta.2010.10.093.

[22] I. Herraiz-Cardona, E. Ortega, J.G. Antón, V. Pérez-Herranz, Assessment of the roughness factor effect and the intrinsic catalytic activity for hydrogen evolution reaction on Ni-based electrodeposits, Int. J. Hydrogen Energy. 36 (2011) 9428–9438. doi:10.1016/j.ijhydene.2011.05.047.

[23] R. Solmaz, G. Kardaş, Electrochemical deposition and characterization of NiFe coatings as electrocatalytic materials for alkaline water electrolysis, Electrochim. Acta. 54 (2009) 3726–3734. doi:10.1016/j.electacta.2009.01.064.

[24] Y. Ullal, A.C. Hegde, Electrodeposition and electro-catalytic study of nanocrystalline Ni–Fe alloy, Int. J. Hydrogen Energy. 39 (2014) 10485–10492. doi:10.1016/j.ijhydene.2014.05.016.

[25] R. Solmaz, A. Döner, G. Kardaş, The stability of hydrogen evolution activity and corrosion behavior of NiCu coatings with long-term electrolysis in alkaline solution, Int. J. Hydrogen Energy. 34 (2009) 2089–2094. doi:10.1016/j.ijhydene.2009.01.007.

[26] S.H. Ahn, H.-Y. Park, I. Choi, S.J. Yoo, S.J. Hwang, H.-J. Kim, E. Cho, C.W. Yoon, H. Park, H. Son, J.M. Hernandez, S.W. Nam, T.-H. Lim, S.-K. Kim, J.H. Jang, Electrochemically fabricated NiCu alloy catalysts for hydrogen production in alkaline water electrolysis, Int. J. Hydrogen Energy. 38 (2013) 13493–13501. doi:10.1016/j.ijhydene.2013.07.103.

[27] C. Fan, D.L. Piron, A. Sleb, P. Paradis, Study of Electrodeposited Nickel-Molybdenum, Nickel-Tungsten, Cobalt-Molybdenum, and Cobalt-Tungsten as Hydrogen Electrodes in Alkaline Water Electrolysis, J. Electrochem. Soc. 141 (1994) 382. doi:10.1149/1.2054736.

[28] M.A. Oliver-Tolentino, E.M. Arce-Estrada, C.A. Cortés-Escobedo, A.M. Bolarín-Miro, F. Sánchez-De Jesús, R. de G. González-Huerta, A. Manzo-Robledo, Electrochemical behavior of NixW1−x materials as catalyst for hydrogen evolution reaction in alkaline media, J. Alloys Compd. 536 (2012) S245–S249. doi:10.1016/j.jallcom.2011.12.086.

[29] E. Lamy-Pitara, J. Barbier, The electrocatalytic reactions of oxidation and evolution of hydrogen on iridium electrodes modified by sulphur adsorption, J. Electroanal. Chem. 416 (1996) 47–51. doi:10.1016/S0022-0728(96)04717-1.

[30] B. Łosiewicz, A. Budniok, E. Rówiński, E. Łągiewka, A. Lasia, The structure, morphology and electrochemical impedance study of the hydrogen evolution reaction on the modified nickel electrodes, Int. J. Hydrogen Energy. 29 (2004) 145–157. doi:10.1016/S0360-3199(03)00096-X.

[31] A. Döner, E. Taşkesen, G. Kardaş, Hydrogen evolution stability of platinum modified graphite electrode, Int. J. Hydrogen Energy. 39 (2014) 11355–11359. doi:10.1016/j.ijhydene.2014.05.159.

[32] A.M. Mohammad, M.I. Awad, M.S. El-Deab, T. Okajima, T. Ohsaka, Electrocatalysis by nanoparticles: Optimization of the loading level and operating pH for the oxygen evolution at crystallographically oriented manganese oxide nanorods modified electrodes, Electrochim. Acta. 53 (2008) 4351–4358. doi:10.1016/j.electacta.2008.01.081.

[33] M.A. Amin, S.A. Fadlallah, G.S. Alosaimi, In situ aqueous synthesis of silver nanoparticles supported on titanium as active electrocatalyst for the hydrogen evolution reaction, Int. J. Hydrogen Energy. 39 (2014) 19519–19540. doi:10.1016/j.ijhydene.2014.09.100.

[34] X. Huang, M. Xie, Y. Chen, Q. Zong, Z. Liu, Y. Jin, Copper–silver oxide nanowires grown on an alloy electrode as an efficient electrocatalyst for water oxidation, RSC Adv. 5 (2015) 26150–26156. doi:10.1039/C5RA00820D.

[35] M.A. Amin, S.A. Fadlallah, G.S. Alosaimi, F. Kandemirli, M. Saracoglu, S. Szunerits, R. Boukherroub, Cathodic activation of titanium-supported gold nanoparticles: An efficient and stable electrocatalyst for the hydrogen evolution reaction, Int. J. Hydrogen Energy. 41 (2016) 6326–6341. doi:10.1016/j.ijhydene.2016.02.107.

[36] J.M. McEnaney, T.L. Soucy, J.M. Hodges, J.F. Callejas, J.S. Mondschein, R.E. Schaak, Colloidally-synthesized cobalt molybdenum nanoparticles as active and stable electrocatalysts for the hydrogen evolution reaction under alkaline

conditions, J. Mater. Chem. A. 4 (2016) 3077–3081. doi:10.1039/C5TA07055D.
[37] X. Yu, M. Wang, Z. Wang, X. Gong, Z. Guo, 3D multi-structural porous NiAg films with nanoarchitecture walls: high catalytic activity and stability for hydrogen evolution reaction, Electrochim. Acta. 211 (2016) 900–910. doi:10.1016/j.electacta.2016.06.062.
[38] C. González-Buch, I. Herraiz-Cardona, E.M. Ortega, S. Mestre, V. Pérez-Herranz, Synthesis and characterization of Au-modified macroporous Ni electrocatalysts for alkaline water electrolysis, Int. J. Hydrogen Energy. 41 (2016) 764–772. doi:10.1016/j.ijhydene.2015.10.142.
[39] T. Klaus, R. Joerger, E. Olsson, C.G. Granqvist, Silver-based crystalline nanoparticles, microbially fabricated., Proc. Natl. Acad. Sci. U. S. A. 96 (1999) 13611–4. doi:10.1073/PNAS.96.24.13611.
[40] S. Anil Kumar, M.K. Abyaneh, S.W. Gosavi, S.K. Kulkarni, R. Pasricha, A. Ahmad, M.I. Khan, Nitrate reductase-mediated synthesis of silver nanoparticles from AgNO3, Biotechnol. Lett. 29 (2007) 439–445. doi:10.1007/s10529-006-9256-7.
[41] C.Y. Flores, C. Diaz, A. Rubert, G.A. Benítez, M.S. Moreno, M.A. Fernández Lorenzo de Mele, R.C. Salvarezza, P.L. Schilardi, C. Vericat, Spontaneous adsorption of silver nanoparticles on Ti/TiO2 surfaces. Antibacterial effect on Pseudomonas aeruginosa, J. Colloid Interface Sci. 350 (2010) 402–408. doi:10.1016/j.jcis.2010.06.052.
[42] C. Marozzi, A. Chialvo, Development of electrode morphologies of interest in electrocatalysis. Part 1: Electrodeposited porous nickel electrodes, Electrochim. Acta. 45 (2000) 2111–2120. doi:10.1016/S0013-4686(99)00422-3.
[43] A. Rami, A. Lasia, Kinetics of hydrogen evolution on Ni-Al alloy electrodes, J. Appl. Electrochem. 22 (1992) 376–382. doi:10.1007/BF01092692.
[44] E. Navarro-Flores, Z. Chong, S. Omanovic, Characterization of Ni, NiMo, NiW and NiFe electroactive coatings as electrocatalysts for hydrogen evolution in an acidic medium, J. Mol. Catal. A Chem. 226 (2005) 179–197. doi:10.1016/j.molcata.2004.10.029.
[45] L. Birry, A. Lasia, Studies of the Hydrogen Evolution Reaction on Raney Nickel–Molybdenum Electrodes, J. Appl. Electrochem. 34 (2004) 735–749. doi:10.1023/B:JACH.0000031161.26544.6a.
[46] L. Bai, D.A. Harrington, B.E. Conway, Behavior of overpotential—deposited species in Faradaic reactions—II. ac Impedance measurements on H2 evolution kinetics at activated and unactivated Pt cathodes, Electrochim. Acta. 32 (1987) 1713–1731. doi:10.1016/0013-4686(87)80006-3.
[47] N.A. Assunção, M.J. de Giz, G. Tremiliosi-Filho, E.R. Gonzalez, A Study of the Hydrogen Evolution Reaction on a Ni/NiFeS Electrodeposited Coating, J. Electrochem. Soc. 144 (1997) 2794. doi:10.1149/1.1837897.
[48] G.J. Brug, A.L.G. van den Eeden, M. Sluyters-Rehbach, J.H. Sluyters, The analysis of electrode impedances complicated by the presence of a constant phase element, J. Electroanal. Chem. Interfacial Electrochem. 176 (1984) 275–295. doi:10.1016/S0022-0728(84)80324-1.

Table 1. Profile of the current density applied for silver nanoparticles electrodeposition.

	E1	E2	E3
t_{ramp} (s)	10	70	10
t_{const} (s)	60	30	170
Q (C)	0.00325	0.00325	0.00875
m_{Ag} ($mg \cdot cm^{-2}$)	0.00727	0.00727	0.0196

Table 2. Kinetic parameters of the HER obtained from the polarization curves recorded in 30 wt.% KOH solution at different temperatures.

Electrode		Temperature		
		30	50	80
Macroporous Ni	b (mV·dec^{-1})	-102	-125	-142
	i_0 (mA·cm^{-2})	0.23	0.41	1.90
	α	0.59	0.51	0.42
	η_{100} (mV)	345	298	268
E1	b (mV·dec^{-1})	-89	-93	-114
	i_0 (mA·cm^{-2})	0.19	0.53	1.38
	α	0.67	0.69	0.52
	η_{100} (mV)	314	214	217
E2	b (mV·dec^{-1})	-95	-96	-110
	i_0 (mA·cm^{-2})	0.22	0.50	1.85
	α	0.63	0.67	0.64
	η_{100} (mV)	267	210	206
E3	b (mV·dec^{-1})	-134	-113	-155
	i_0 (mA·cm^{-2})	1.15	1.47	2.93
	α	0.45	0.57	0.36
	η_{100} (mV)	260	207	244

Table 3. EEC parameters obtained by fitting EIS experimental spectra recorded in 30 wt.% KOH solutions.

		χ^2	Rs ($\Omega \cdot cm^2$)	R_1 ($\Omega \cdot cm^2$)	Q_1 ($m\Omega^{-1} \cdot cm^{-2} \cdot s^n$)	n_1	C_1 ($mF \cdot cm^{-2}$)	R_2 ($\Omega \cdot cm^2$)	Q_2 ($m\Omega^{-1} \cdot cm^{-2} \cdot s^n$)	n_2	C_2 ($mF \cdot cm^{-2}$)	R_f
η (mV)	0	$2.55 \cdot 10^{-4}$	0.5	21.86	18.61	0.9	11.09	33.68	32.25	0.57	1.36	554.74
	47	$2.46 \cdot 10^{-4}$	0.51	16.38	14.16	0.91	8.44	9.97	49.8	0.72	11.39	422.17
	95	$2.16 \cdot 10^{-4}$	0.53	6.29	11.63	0.9	6.71	0.83	373.17	0.91	304.26	335.71
	150	$1.79 \cdot 10^{-4}$	0.5	2.12	10.36	0.87	4.56					227.96
T (ºC)	30	$1.27 \cdot 10^{-4}$	0.81	52.18	36.34	0.92	26.93	5.74	24.01	1	24.01	1346.31
	50	$6.36 \cdot 10^{-4}$	0.7	30.85	33.72	0.93	25.78	2.83	30.03	1	30.03	1289.11
	80	$5.30 \cdot 10^{-4}$	0.51	13.95	31.9	0.91	21.53					1076.71
Electrode	Ni	$4.74 \cdot 10^{-4}$	0.56	59.17	16.72	0.93	12	17.65	294.36	0.76	166.55	600.22
	E1	$2.55 \cdot 10^{-4}$	0.5	21.86	18.61	0.9	11.09	33.68	32.25	0.57	1.36	554.74
	E2	$6.36 \cdot 10^{-4}$	0.7	30.85	33.72	0.93	25.78	2.83	30.03	1	30.03	1289.11
	E3	$7.96 \cdot 10^{-4}$	0.64	20.02	55.64	0.94	44.68					2233.97

A B

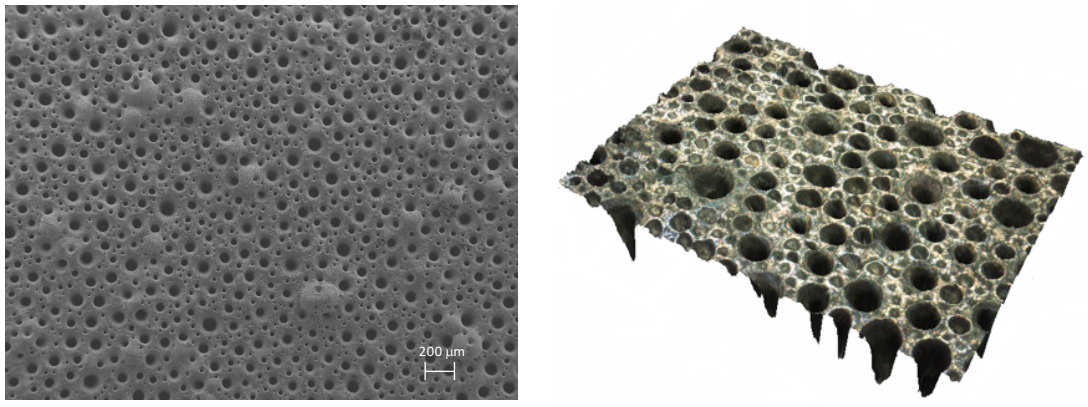

Figure 1. FE-SEM images of the macroporous Ni electrode (A) and 3D confocal laser micrograph (B).

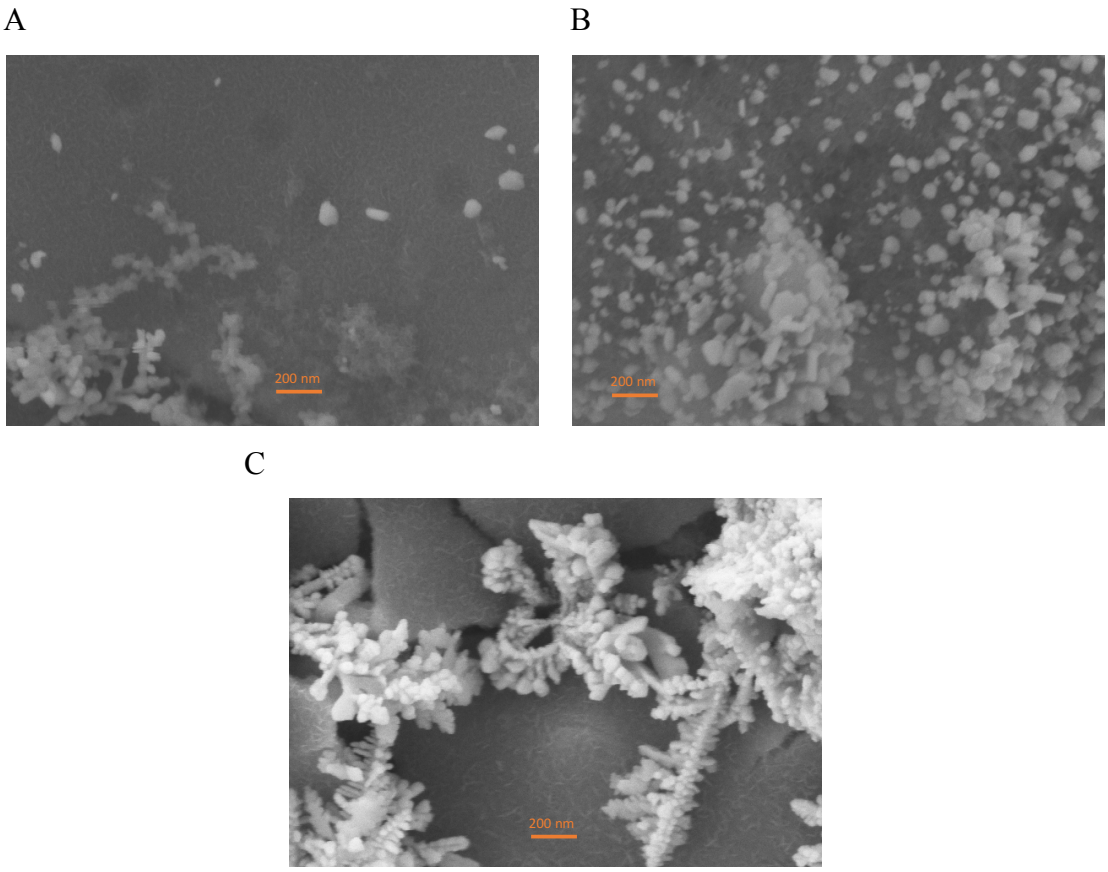

Figure 2. FE-SEM images of silver nanoparticles deposited on the electrode's surface. Electrode E1 (A), electrode E2 (B), electrode E3 (C).

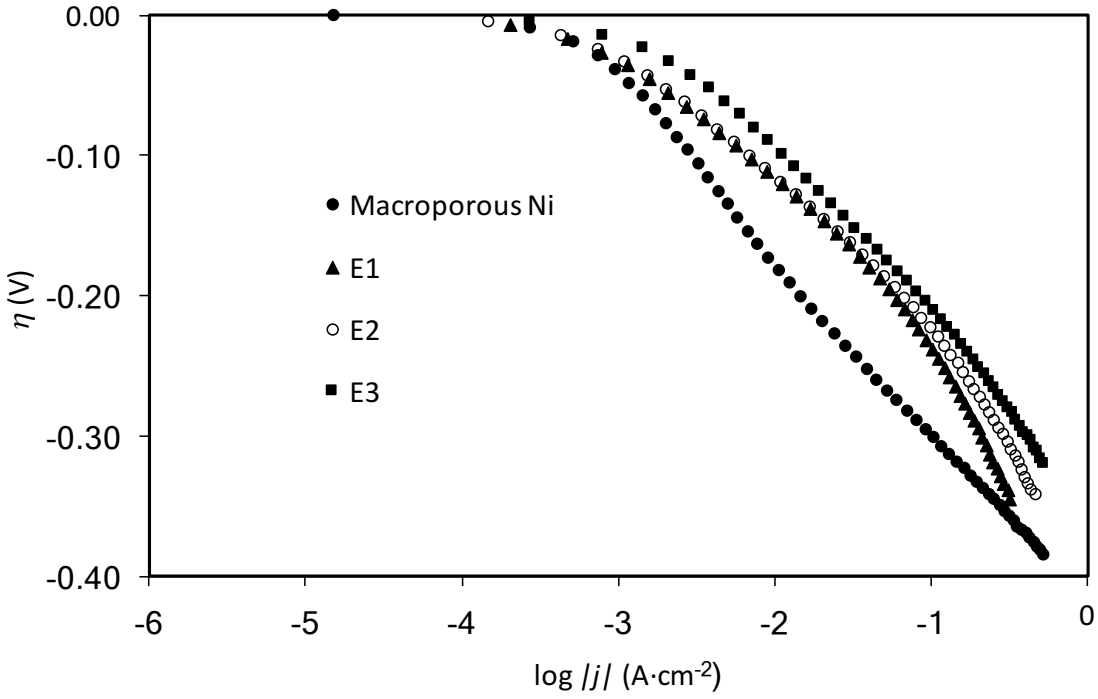

Figure 3. Linear Tafel polarization curves recorded on the investigated electrodes in 30 wt.% KOH solution at 50ºC.

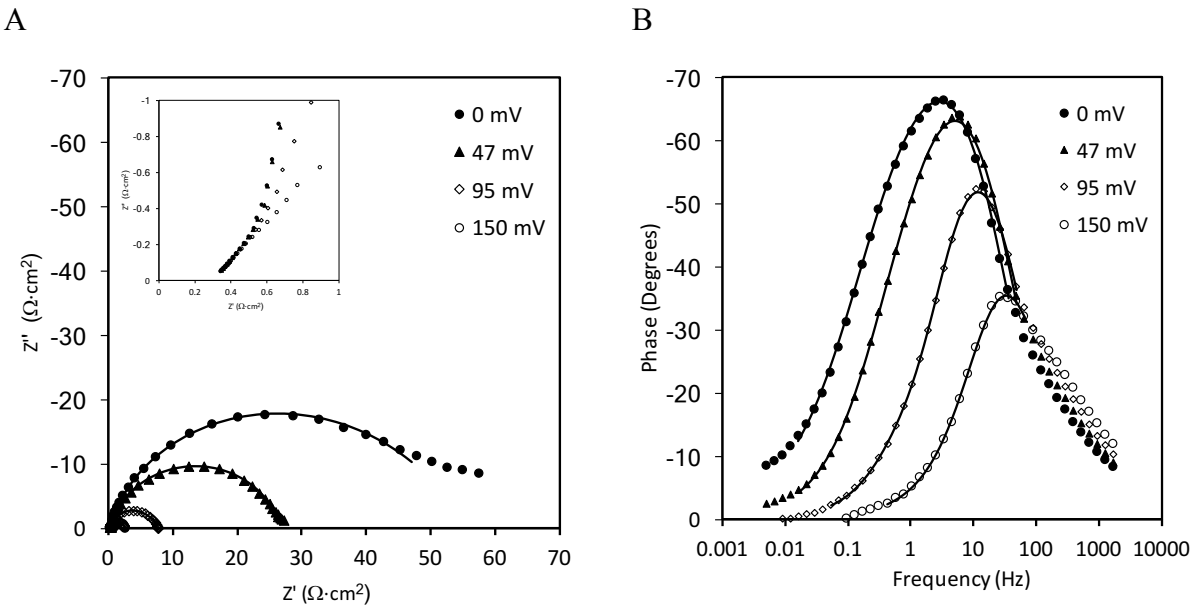

Figure 4. Impedance data obtained in 30 wt.% KOH solution at 50ºC for electrode E1. A. Nyquist representation, B. Bode representation of the phase angle as a function of frequency. Symbols are the experimental points and solid lines are modelled data.

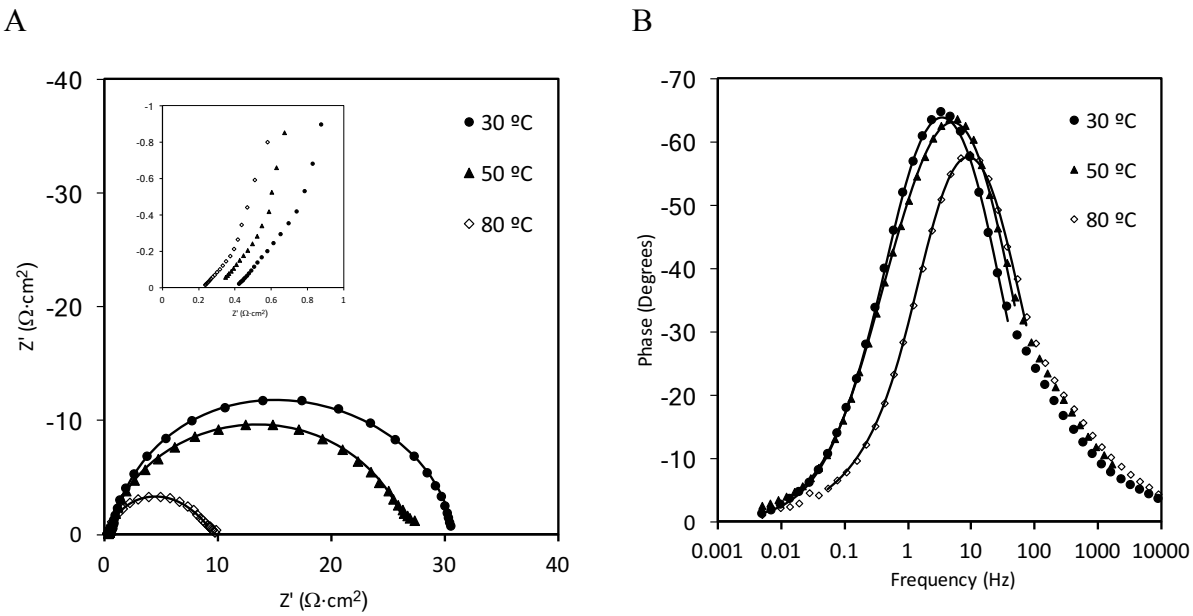

Figure 5. Impedance data obtained in 30 wt.% KOH solution at an overvoltage of 50 mV for electrode E1. A. Nyquist representation, B. Bode representation of the phase angle as a function of frequency. Symbols are the experimental points and solid lines are modelled data.

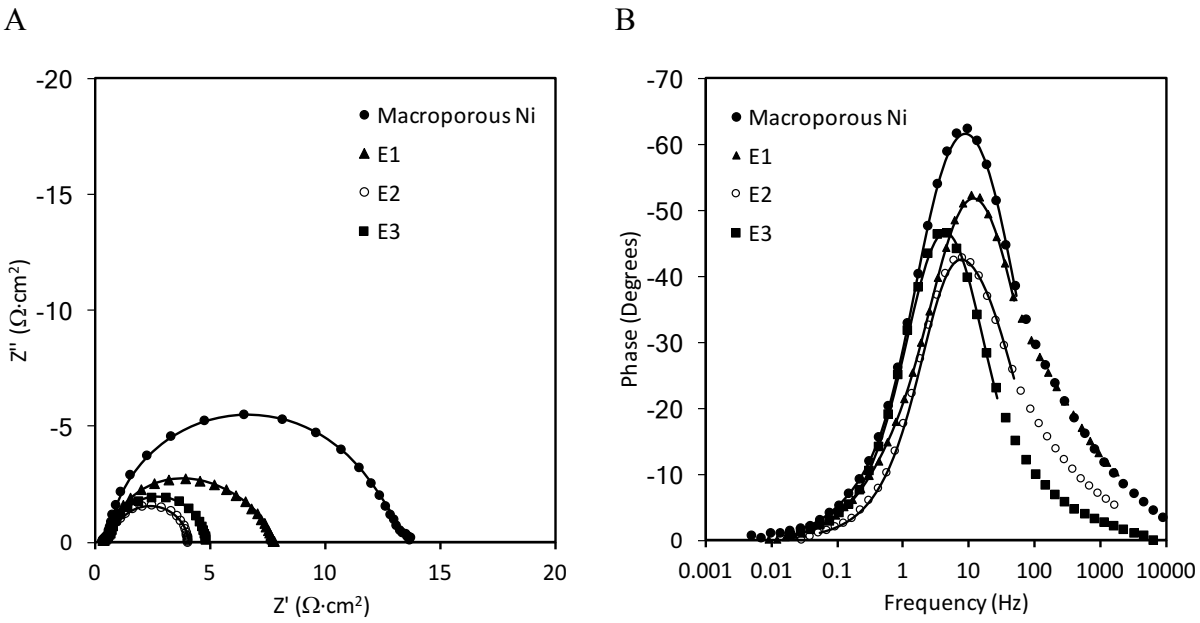

Figure 6. Impedance data obtained in 30 wt.% KOH solution at an overvoltage of 100 mV and 50 ºC for the developed electrodes. A. Nyquist representation, B. Bode representation of the phase angle as a function of frequency. Symbols are the experimental points and solid lines are modelled data.

A

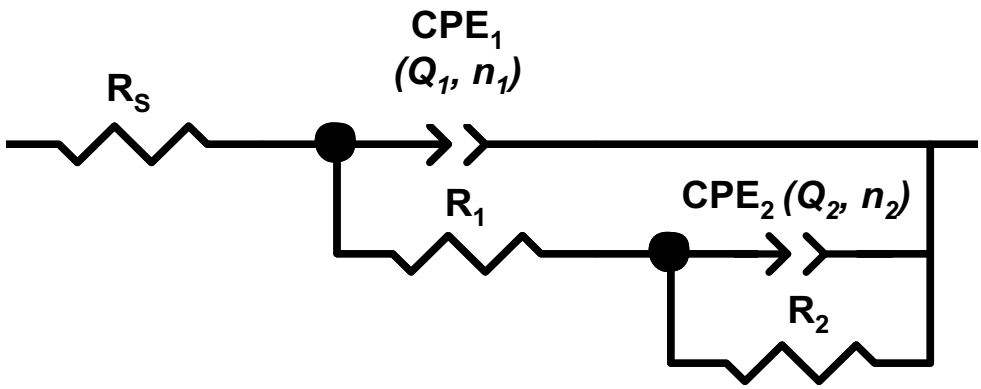

B

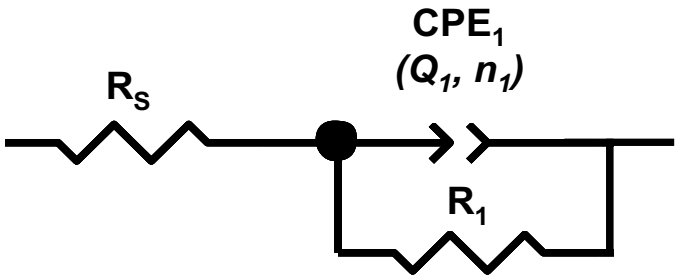

Figure 7. EEC models used to explain the EIS response of the HER on the developed electrocatalysts: A. two-time constant parallel model (2TP), and B. one-time constant (1T).

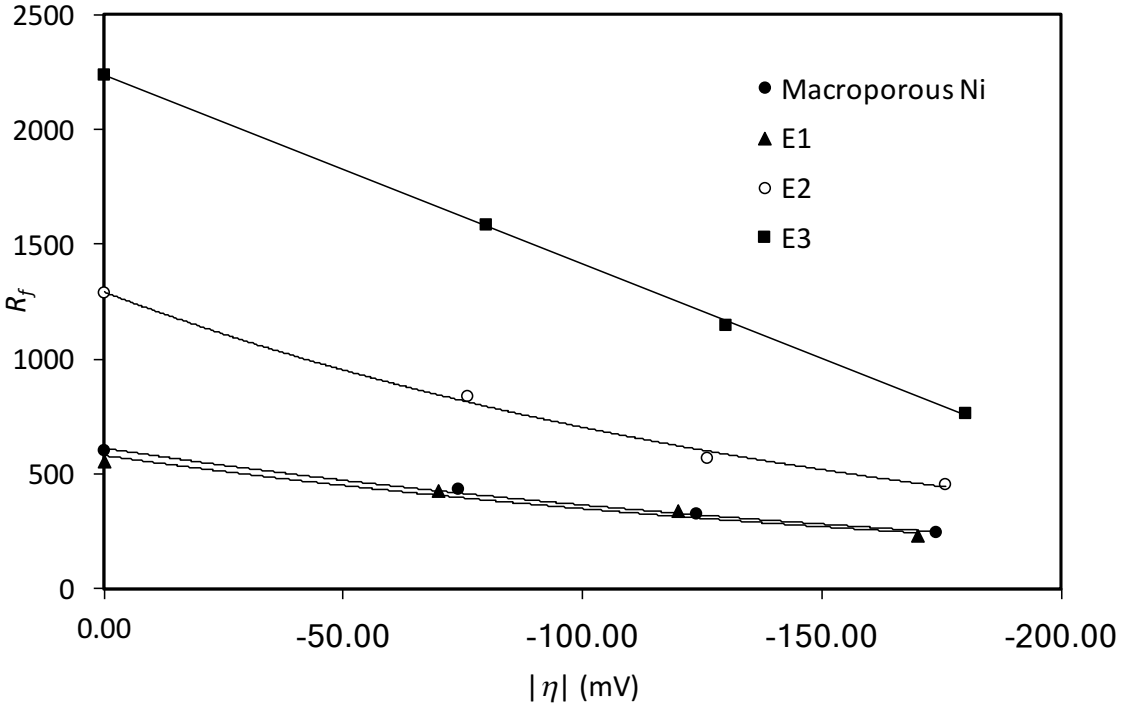

Figure 8. Surface roughness factor, R_f, as a function of the overpotential for the developed electrodes at 50 ºC.

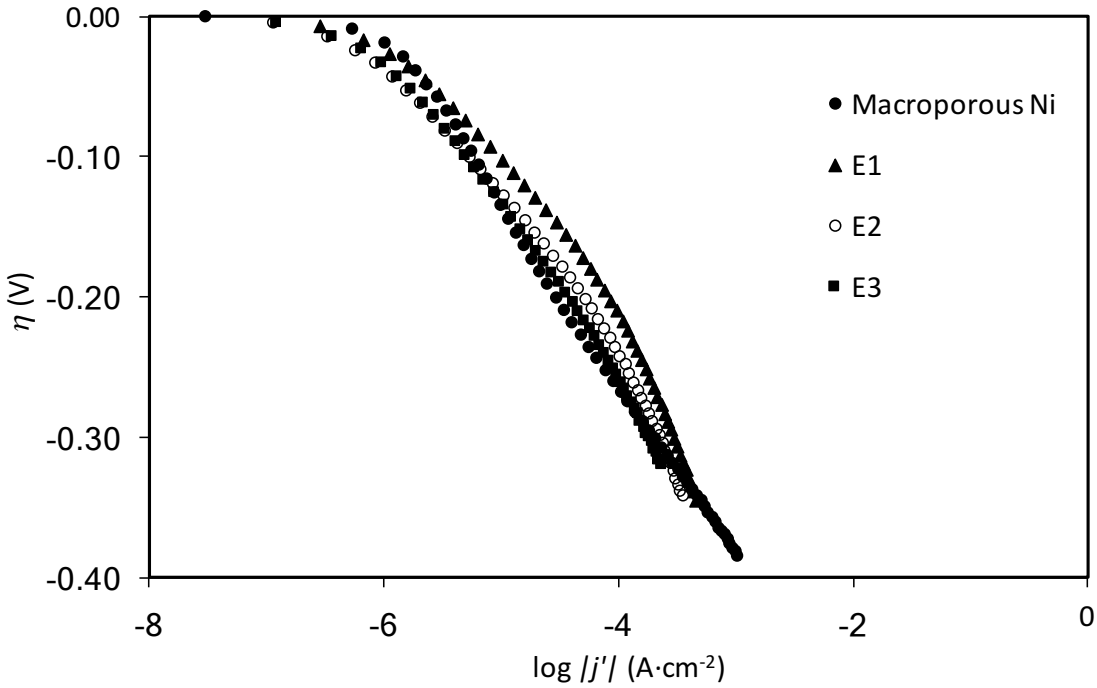

Figure 9. Linear Tafel polarization curves recorded on the investigated electrodes in 30 wt.% KOH solution at 50ºC, corrected considering the roughness factor, R_f.